Supplementary Materials for

T cell costimulatory receptor CD28 is a primary target for PD-1–mediated inhibition

Enfu Hui, Jeanne Cheung, Jing Zhu, Xiaolei Su, Marcus J. Taylor, Heidi A. Wallweber, Dibyendu K. Sasmal, Jun Huang, Jeong M. Kim, Ira Mellman,* Ronald D. Vale*

*Corresponding author. Email: ron.vale@ucsf.edu (R.D.V.); mellman.ira@gene.com (I.M.)

Published 9 March 2017 on *Science* First Release
DOI: 10.1126/science.aaf1292

This PDF file includes:

Other Supplementary Material for this manuscript includes the following:
(available at www.sciencemag.org/cgi/content/full/science.aaf1292/DC1)

Materials and Methods

Reagents:

Advance RPMI 1640 (#12633), 100× Penicillin-Streptomycin-Glutamine (#10378016), Lipofectamine 2000 (#11668027), and Dynabeads® Protein G (#10004) were purchased from Thermo Fisher Scientific. Heat inactivated fetal bovine serum were obtained from Hyclone. Synthetic 1,2-dioleyl-sn-glycero-3-phosphocholine (POPC), 1-palmitoyl-2-oleoyl-*sn*-glycero-3-phospho-L-serine (POPS), 1,2-dioleoyl-sn-glycero-3-[(N-(5-amino-1-carboxypentyl)iminodiacetic acid)succinyl] (nickel salt, DGS-NTA-Ni), N-(lissamine rhodamine B sulfonyl)-1,2-dipalmitoyl-sn-glycero-3 phosphoethanolamine (Rhodamine-PE), and 1,2-dioleoyl-sn-glycero-3-phosphoethanolamine-N-[methoxy(polyethylene glycol)-5000] (ammonium salt) (PEG5000 PE) were purchased from Avanti Polar Lipids. SNAP-Cell-505 (#S9103) was purchased from New England Biolabs. Apyrase (#A6535) and Polyethylenimine (#408727) were obtained from Sigma-Aldrich.

Recombinant Proteins

The extracellular domain of mouse MHC class I molecule H2Kb was expressed as a disulfide stabilized single chain trimer with a covalently linked ovalbumin (OVA) peptide SIINFEKL (*48*), and a His_{10} tag engineered to the C-terminus, in the Bac-to-Bac baculovirus expression system (Thermo Fisher Scientific). His_{10}-tagged extracellular domains of recombinant human B7.1, ICOSL and PD-L1 were obtained from Sino Biologicals. Human protein tyrosine kinase Lck (with a G2A mutation to abolish myristoylation), the cytosolic portion of the TCR signaling subunit CD3ζ (aa 52-164), and the cytosolic portion of the protein tyrosine phosphatase CD45 (aa 598-1304) were all expressed and purified with an N-terminal His_{10} tag as described (*40*). The cytosolic tails of human PD-1 (aa 194-288), CD28 (aa 180-220), ICOS (aa 162-199), CD3ε (aa 153-207), DAP10 (aa 70-92), CTLA4 (aa 183-223), CD226 (aa 288-336), CD96 (aa 541-569) and TIGIT (aa 163-244) were expressed with an N-terminal His_{10}-tag in *Escherichia coli* using the pET28a vector. Human full length protein tyrosine kinase ZAP70 and Csk, protein tyrosine phosphatase Shp1 and Shp2, lipid phosphatase SHIP-1, and regulatory subunit of PI3K (p85α) were all expressed with an N-terminal Glutathione S-transferase (GST) tag followed by a PreScission recognition sequence (LEVLFQGP), and a SNAP-Tag in the Bac-to-Bac baculovirus expression system. The tandem SH2 domains of human Shp1 and Shp2, and the adaptor protein human Grb2 were bacterially expressed with an N-terminal GST tag followed by a PreScission recognition sequence (LEVLFQGP), and a SNAP-Tag via pGEX6P-1 vector. For attaching Shp2 onto LUV membranes in **fig. S4**, full length Shp2 with an N-terminal His_{10} tag were expressed in SF9 cells via the Bac-to-Bac baculovirus system. Human LAT (aa 48-233) with an N-terminal His_8 tag, Gads (aa 1-155 and 261-330) with an internal GB1 tag and SLP-76 (aa 101-420) were expressed in *Escherichia coli* and purified as described (*49*). All GST fusion proteins were purified using Glutathione Sepharose 4B. The GST tag were subsequently removed via the PreScission protease (GE Healthcare), as described previously (*40*). All poly-histidine tagged proteins were purified using the Ni-NTA agarose (GE Healthcare), and eluted with imidazole. All affinity purified proteins were subjected to gel filtration chromatography using HEPES buffered saline (50 mM HEPES-NaOH, pH 7.5, 150 mM NaCl, 10% glycerol, 1 mM TCEP). The monomer fractions were pooled, aliquoted, snap frozen and stored at -80 °C.

Primary CD8+ T Cells

Splenocytes were harvested from C57BL/6-Tg (TcraTcrb) 1100Mjb/J (OT-1) mice (Jackson Laboratory) and CD8 cells were purified by negative selection using the mouse CD8a+ T cell isolation kit from Milteny Biotec (#130-104-075, Auburn, CA).

Jurkat T Cells and Raji B Cells

Jurkat E6.1 T cells and Raji B cell were a generous gift from Arthur Weiss (UCSF). Raji B cells were obtained from Michael McManus (UCSF). Both cell lines were maintained in RPMI medium (advanced RPMI 1640 supplemented with 10% fetal bovine serum, 10 mM HEPES, 1x Penicillin-Streptomycin-Glutamine).

Retrovirus Production and Transduction

For imaging experiments shown in **Fig. 3**, the OT-I cells were retrovirally transduced to express fluorescently tagged proteins. For this purpose, cDNAs encoding mouse PD-1–mCherry, CD28–mGFP was cloned into the pMSCV vector, and co-transfected with pCl-Eco packaging plasmid into Phoenix-Eco retrovirus packaging cell line using Lipofectamine 2000 (Thermo Fisher Scientific) per manufacturer's instructions. Virus supernatants were harvested at 48 h and 72 h after transfection. Freshly purified OT-I cells were stimulated with anti-CD3 (5 μg/ml), anti-CD28 (3 μg/ml) in RPMI medium supplemented with 100 U/ml mouse recombinant IL-2 and 5 mM β-mecaptoethanol at 37 °C / 5% CO_2 incubator. 36 hours after stimulation, OT-I cells were overlaid with freshly harvested retrovirus supernatants containing 8 μg/ml Lipofectamine and 100 U/ml mouse recombinant IL-2, spin-infected at 35 °C, 1000× g for 60 min, and incubated at 37 °C / 5% CO_2 overnight. The virus supernatant was replaced with fresh T cell culture medium the second day and cells incubated for another 48–96 hours before microscopy.

Lentivirus Production and Transduction

For Raji B cells mediated T cell stimulation assays, human PD-L1 and PD-1 were introduced into Raji and Jurkat respectively via lentiviral transduction. To produce lentiviruses, cDNA encoding the gene of interest was cloned into the pHR vector, and co-transfected with the envelop plasmid pMD2.G and the packaging plasmid p8.91 into HEK293T cells using Polyethylenimine in DMEM medium. After 18 hours incubation at 37 °C incubator, the medium was replaced with complete RPMI medium and the virus supernatants harvested 72 hours after transfection. To transduce Jurkat T cells, 0.5 million cells were pelleted at 600× g for 4 min and resuspended in 1 ml of fresh virus supernatant, and incubated overnight at 37 °C /5% CO_2 before adding another 9 ml of complete RPMI medium. To transduce Raji B cells, 0.5 million cells were pelleted at 600 x g for 4 min and resuspended in 1 ml of fresh virus supernatant containing 8 μg/ml Lipofectamine in a 24-well plate. The virus–cell mixture was centrifuged at 35 °C, 1000× g for 60 min, and incubated at 37 °C / 5% CO_2 overnight before transferred into a T25 flask containing 9 ml fresh complete RPMI medium. The transduced cells were sorted out via fluorescence activated cell sorting (FACS) at least one week after the lentiviral transduction.

Quantification of PD-1 and CD28 by Flow Cytometry

The surface expression levels of PD-1 and CD28 were quantified using BD Quantibrite™ beads (BD Biosciences), following manufacturer's instructions. Samples were run on either a BD Biosciences FacsCalibur or Fortessa flow cytometer, and analyzed with FlowJo software (TreeStar) and GraphPad Prism.

To obtain activated mouse T cells, a 96 well U-bottom plate was pre-coated with anti-CD3 (BD Biosciences #553057) overnight at 10 μg/ml and washed prior to cell addition. Pan T cells were isolated from C57BL/6 mouse spleens (Charles River Labs) using a negative selection kit (Miltenyi Biotec #130-095-130). T cells were plated in triplicate wells in anti-CD3 coated plates at 0.2 million per well plus 1 μg/ml soluble anti-CD28 (BD Biosciences #553294) overnight. Cells were harvested and stained with CD8 FITC (BD Biosciences #553031), CD4 APC (BD Biosciences #553051), and PD-1 PE (BioLegend #109104) and run on a BD FacsCalibur.

To obtain tumor-infiltrating T cells, 0.1 million CT26 colorectal tumor cells (ATCC) were inoculated subcutaneously into the flanks of Balb/c mice (Charles River Labs). Approximately 12 days later, tumors from individual mice were harvested, minced, and digested for 15 min at 37 °C with 0.5 mg/ml collagenase D (Roche #11088858001) plus 0.1 mg/ml DNAse I (Roche #10104159001) on a rocking platform. Cell suspensions were filtered, washed, and stained with: Near-Infrared Viability dye (Life Technologies #L10119), CD45 v500 (BD Biosciences #561487), CD8 APC (BD Biosciences #553035), CD4 PE-Cy7 (BD Biosciences #552775), Thy1.2 eFluor450 (eBioscience #48-0902), and PD-1 PE (BioLegend #109104).

LCMV clone 13 was inoculated in 8-10 weeks old C57BL/6 mice intraveneously at 2 million pfu per mouse in PBS. Spleens from individual mice were harvested approximately 140 days later and single cell suspensions were stained with PD-1 PE (BioLegend #109104), CD4 APC (BD Biosciences #553051), CD8 Pacific Blue (BD Biosciences #558106), and Thy1.2 PerCp-eFluor710 (eBioscience #46-0903).

Transfected and parental Jurkat and Raji cell lines were stained with PD-1 PE (eBioscience #12-9969), CD28 PE (BD #555729), and PD-L1 PE (eBioscience #12-5983).

Quantification of PD-L1 Expression of *ex vivo* MC38 Tumors and Spleens

C57BL/6 female mice (Charles River Labs) were inoculated subcutaneously with 0.1 million MC38 tumor cells (Genentech internal cell bank) in the hind flank. Tumors and spleens were harvested 28 days later. Tumor cells were dissociated using a mouse tumor dissociation kit (Miltenyi #130-096-730) according to the manufacturer's instructions. Spleens were made into single cell suspensions and filtered. Cells were stained with NIR-Infared viability dye (Life Technologies #L10119), PD-L1 PE (BD Biosciences#558091), CD45 v500 (BD Biosciences #561487), CD4 APC (BD Biosciences #553051), CD8 PerCp-Cy5.5 (BD Biosciences #551162), CD11b FITC (BD Biosciences #553310), Ly6C eFluor450 (eBioscience #48-5932), Ly6G PE-Cy7 (BioLegend #127618), and F4/80 Alexa700 (BioLegend #123130). Macrophages were identified as CD45+ CD11b+ Ly6C- Ly6G- F4/80+. Monocyte-derived suppressor cells (tumors) and monocytes (spleen) were identified as CD45+ CD11b+ Ly6C+ Ly6G-. Granulocytic-monocytes-derived suppressor cells (tumors) and neutrophils (spleen) were identified as CD45+ CD11b+ Ly6C- Ly6G+. MC38 tumor cells were identified as CD45-.

Small Unilamellar Vesicles (SUVs)

Phospholipids (98% POPC, 2% DGS-NTA-Ni and 0.1% PEG5000 PE) were dried under a stream of Argon, desiccated for at least 1 hour and suspended in 1× phosphate buffered saline (PBS, pH 7.4). Small unilamellar vesicles (SUVs) were formed via 20 freeze-thaw cycles of the lipid suspension, which were then subjected to centrifugation at 33,500× g for 45 min at 4 °C using a

TLA120 rotor (Beckman Coulter) to remove multilamellar vesicles. Supernatant containing SUVs was collected and proceed immediately to the formation of supported lipid bilayer.

Large Unilamellar Vesicles (LUVs)
Phospholipids (79.7% POPC + 10% POPS + 10% DGS-NTA-Ni + 0.3% Rhodamine-PE) were dried under a stream of Argon, desiccated for at least 1 hour and suspended in 1x Reaction buffer (50 mM HEPES-NaOH, pH 7.5, 150 mM NaCl, 10 mM $MgCl_2$, 1 mM TCEP). LUVs were prepared by extrusion 20 times through a pair of polycarbonate filters with a pore size of 200 nm, as described previously (*40*).

Supported Lipid Bilayer
The supported lipid bilayers (SLBs) were formed in 96-well glass-bottomed plates (Matrical). Glass was washed with Hellmanex III (Hëlma Analytics) for 3 hours at 50 °C, thoroughly rinsed with ddH_2O, washed twice with 5 M KOH for 15 min, and thoroughly rinsed with ddH2O followed by equilibration with PBS. Freshly prepared SUVs were added to cleaned wells containing PBS. Wells were incubated for 1 hour at 50 °C to induce SLB formation, and then thoroughly washed with PBS to remove excess SUVs. SLBs were blocked with 1 mg/mL BSA in PBS for 30 min at room temperature. His_{10}-tagged T cell ligands were premixed and overlaid onto SLBs. After 30 min incubation at 37 °C, the unbound proteins were washed away with excess PBS, incubated for another 30 min, and washed again with imaging buffer (20 mM HEPES-NaOH, pH 7.5, 137 mM NaCl, 5 mM KCl 1 mM $CaCl_2$, 2 mM $MgCl_2$, 0.7 mM Na_2HPO_4, 6 mM D-glucose, and 1% BSA) (*50*).

TIRF Microscopy
OT-I cells co-transduced with mouse PD-1–mCherry and mouse CD28–mGFP or mouse ICOS–mGFP were harvested via centrifugation at 200× g for 4 min, incubated with 10 μg/ml Alexa Fluor 647 labeled H57-597 mouse TCRβ antibody or its single chain variable fragment (*51*) for 30 min on in ice, washed three times with imaging buffer, and then plated onto SLBs functionalized with peptide bound MHC-I (H2Kb-SIINFEKL), ICAM-1, B7.1 and PD-L1. Time-lapse TIRF microscopy images were acquired at 37 °C on a Nikon Eclipse Ti microscope equipped with a 100x Apo TIRF 1.49 NA objective, using a Digital sCMOS camera ORCA-Flash 4.0 C11440 (Hamamatsu Photonics). The microscope was controlled by the Micro-Manager software (*52*). Images were processed and analyzed using ImageJ (Fiji). The Pearson's correlation coefficients were calculated using the "Coloc2" plugin in Fiji. The fold intensity values for the line scan analyses were calculated as described previously (*21*).

LUV Reconstitution and FRET Assays
Experiments were carried as described (*40*), with modifications. Briefly, purified cytosolic domains of the receptor of interest, Lck kinase and SH2 containing cytosolic effectors were pre-mixed at desired ratios in 1x Reaction Buffer (50 mM HEPES-NaOH (pH 7.5), 150 mM NaCl, 10 mM $MgCl_2$, 1 mM TCEP) containing 0.5 mg/ml BSA, and then mixed with LUVs harboring DGS-NTA-Ni and Rhodamine-PE. The proteins-LUVs mixture were loaded onto a solid white, 96-well polystyrene plates (Corning), and continue to incubate at room temperature for 1 hour, during which the SNAP505 fluorescence was monitored using a plate reader with 504-nm excitation and 540-nm emission. During the incubation, His-tagged proteins bound to the liposomes whereas the SH2 effector remained in the extravesicular solution. ATP was then injected followed by 5 sec of

automatic shaking of the plate at medium speed, and the fluorescence was further monitored for a desired period of time. To measure the pure phosphatase activities in **Fig. 1G** and **fig. S4**, the reactions were paused, added with excess ATP scavenger apyrase to rapidly deplete the ATP, and the fluorescence monitored again. For quantification of membrane recruitment, data were normalized by setting the average fluorescence value of the last 10 data points before ATP addition as 100% and background fluorescence as 0%.

LUV Reconstitution and Phosphotyrosine Western Blot

For experiments described in **Fig. 2, fig. S7** and **fig. S8**, proteins of interest were pre-mixed at desired ratios in 1× Reaction Buffer containing 0.5 mg/ml BSA, and then mixed with LUVs (1 mM total lipids). The proteins-LUVs mixture incubated at room temperature for 1 hour, during which the His-tagged proteins bound to the liposomes whereas other proteins remained in the extravesicular solution. 2 mM ATP was then injected and rapidly mixed. The reactions were allowed to proceed at room temperature for 30-60 min, and terminated with SDS sample buffer. The samples were heated at 95 °C for 5 min, and subjected to SDS-PAGE. Proteins were transferred to nitrocellulose membranes using iBlot™ Dry Blotting system (ThermoFisher Scientific). The membranes were blocked with 5% BSA in Tris-buffered saline (pH 7.4) with 0.1% Tween-20, incubated with desired phosphotyrosine specific antibodies, and detected with HRP based enhanced chemiluminescence. The following primary antibodies were used: anti-pY142-CD3ζ (BD Biosciences #558402), anti-pY20 (Santa Cruz Biotechnology #sc-1624, for detection of tyrosine phosphorylated CD28 in reconstitution assays), anti-pY350 (Santa Cruz Biotechnology #sc-18182, for detection of tyrosine phosphorylated ICOS), anti-pY418-Src (BD Biosciences #560095, for detection of pY394-Lck), anti-pY505-Lck (Cell Signaling #2751), anti-pY315-ZAP70 (Abcam #ab60970), anti-pY493-ZAP70 (Cell Signaling #2704), anti-pY171-LAT (Cell Signaling #3581), anti-pY145-SLP76 (Abcam #ab75829). For experiments described in **fig. S9E**, His_{10}-Lck and indicated concentrations of either His_{10}-CD3ζ or His_{10}-CD28 were reconstituted onto LUVs. After ATP addition, the reactions were terminated at 5 min, an empirically determined time point when the kinase reaction was at the initial linear phase. To estimate the initial rates of kinase reactions, a duplicate reaction for the highest substrate concentration (2.64 μM) was run in parallel but terminated at 80 min, an empirically determined time point when both CD3ζ and CD28 are completely phosphorylated. The 5 min samples and 10% of the 80 min samples were run side by side on SDS-PAGE and blotted with generic phosphotyrosine antibody (pY20, Santa Cruz Biotechnology #sc-1624). Molecular density of a given membrane-bound protein was estimated by dividing the total number of the protein by the total surface areas of the liposome particles as described previously (*40*).

Quantification of T Cell Proteins Using Western Blot

For quantifying the copy number of T cell signaling proteins (Lck, Csk and SLP76) shown in **fig. S6**, 10 million Jurkat T cells were centrifuged at 200× g for 4 min, and resuspended in 400 μl ice cold NP40 lysis buffer (125 mM Tris-HCl, pH 7.4, 150 mM NaCl, 1% NP40, 1 mM EDTA, 5% glycerol, Roche cOmplete EDTA free protease inhibitor cocktail) and incubated on ice for 10 min for lysis. The lysate was then mixed with 1.33× sample buffer, boiled for 5 min and subjected to SDS-PAGE and immunoblotted with anti-Lck (1F6, obtained from A. Weiss lab at UCSF), anti-Csk (C74C1, Cell Signaling #4980), or anti-SLP76 (D1R1A, Cell Signaling #70896). Defined moles of a purified recombinant human protein were run in parallel to serve as standards. The resulting blots were quantified using ImageJ to calculate the mass of protein loaded, and protein

copy numbers per cell were calculated according to Avogadro's number, and molecular densities of membrane proteins computed assuming 11.5 μm diameter of Jurkat T cells.

Jurkat Stimulation Using Raji B Cells

For phosphorylation assays shown in **Fig. 4C** and **fig. S14**, Raji B cells were preincubated with 20-30 ng/ml SEE superantigen (Toxin Technology #ET404) in serum free RPMI medium for 30 min at 37 °C. Jurkat T cells were rested in serum free RPMI medium at 37 °C for 3 hours to reduce the phosphorylation background. 11 million antigen loaded Raji B cells and 15 million rested Jurkat T cells were precooled on ice and mixed in a 96-well plate in ice water. The plate was centrifuged at 330× g for 1 min at 4 °C to initiate cell–cell contact, and immediately transferred to a 37 °C water bath. The reactions were then terminated with NP40 lysis buffer supplemented with Roche phosSTOP phosphatase inhibitor cocktail at indicated time points and equal fractions of the lysates were subjected to SDS-PAGE and phosphotyrosine Western Blot, using the following primary antibodies: anti-pY142-CD3ζ (BD Biosciences #558402), anti-pY418-Src (BD Biosciences #560095, for detection of pY394-Lck), anti-pY505-Lck (Cell Signaling #2751), anti-pY315-ZAP70 (Abcam #ab60970), anti-pY493-ZAP70 (Cell Signaling #2704), anti-pY171-LAT (Cell Signaling #3581), anti-pY145-SLP76 (Abcam #ab75829). To create the PD-L1 gradient in **Fig. 4C**, X % of PD-L1^{High} Raji B were mixed with (100 – X) % of PD-L1^{-} parental Raji B. Five mixtures with identical total number of Raji B but increasing X (0, 10, 20, 50 and 100) were used. For IL-2 secretion assays shown in **Fig. 4B**, Raji B cells were pre-loaded with 30 ng/ml SEE superantigen for 45 min at 37 °C, washed and irradiated 10,000 rads prior to coculture. 200,000 Jurkat were cultured with 50,000 Raji in a 96-well U-bottom plate in triplicate wells and supernatants were collected at 24 hours. Human IL-2 was quantified by ELISA (R&D Systems, #DY202-05).

CD28-PI3K Co-Immunoprecipitation

Antibodies that specifically recognize tyrosine phosphorylated CD28 are not commercially available. Hence in this work, co-immunoprecipitation of CD28 with Type-I PI3K, which binds to tyrosine phosphorylated CD28 with its regulatory subunit p85α, was used to probe CD28 phosphorylation in cell lysates, as shown in **Fig. 4** and **fig. S14**. For this purpose, CD28 was immunoprecipitated from the Jurkat – Raji cell lysates using an anti-CD28 antibody (Santa Cruz Biotechnology #sc-1624). Equal fractions of the immunoprecipitates were subjected to SDS-PAGE and Western Blot, and the co-immunoprecipitated PI3K was detected with Western Blot using anti-p85α (Cell Signaling #4292).

Statistical analyses

Statistical significance was evaluated by two-tailed Student's t test except for **Fig. 4B**, which was evaluated by two-way ANOVA due to multiple technical repeats within each independent experiment.

Supplementary Figures

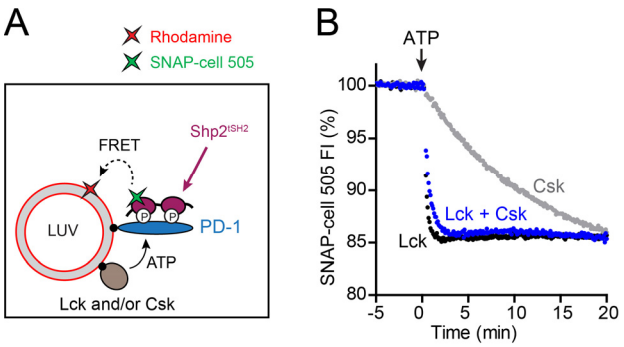

Fig. S1. Comparison of Lck and Csk on their kinase activities towards PD-1.

(**A**) Cartoon of a FRET assay for comparing the abilities of Lck and Csk to phosphorylate PD-1. His_{10}-tagged cytosolic tail of PD-1 (300 nM) was co-attached to Rhodamine-PE bearing LUVs with Lck (100 nM), Csk (100 nM), or both. The SNAP-Cell-505 labeled tandem SH2 domains of Shp2 ($Shp2^{tSH2}$, 200 nM) was presented in the extravesicular solution as a reporter for PD-1 phosphorylation. Addition of ATP allowed the kinase(s) to phosphorylate PD-1, causing membrane recruitment of $Shp2^{tSH2}$ and FRET.

(**B**) Time course of $Shp2^{tSH2}$ fluorescence in response to 1 mM ATP under the three conditions described in **A**: PD-1 + Lck (black), PD-1 + Csk (gray), and PD-1 + Lck + Csk (blue).

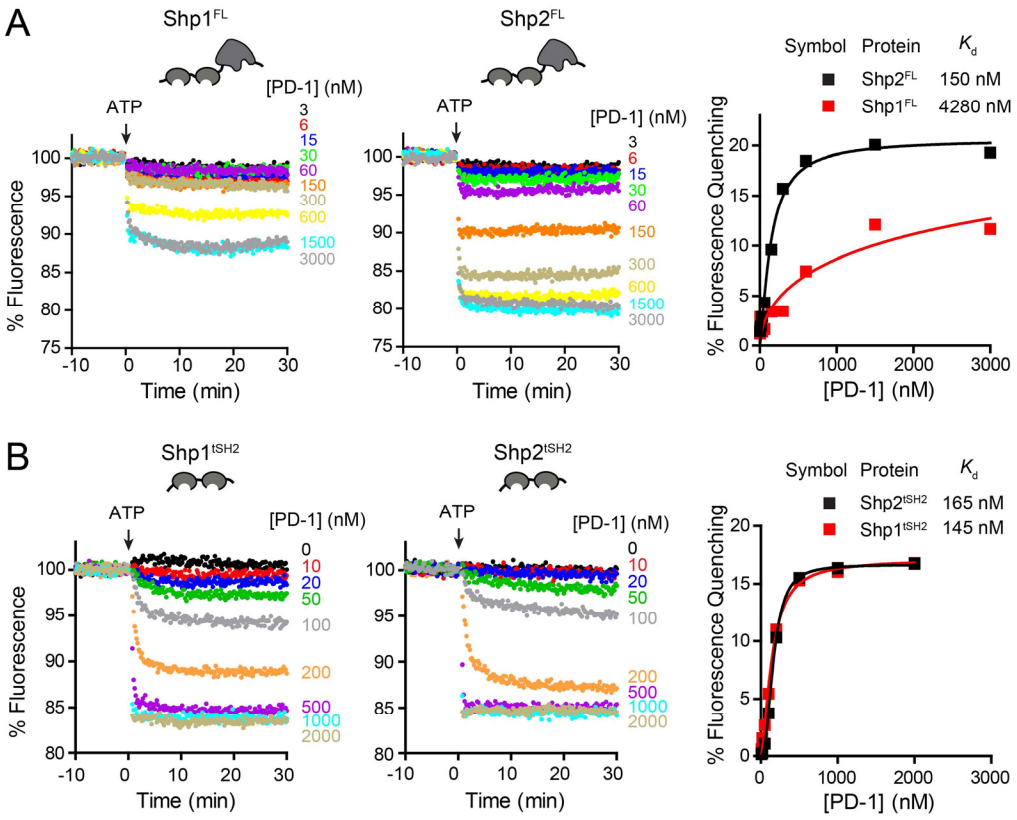

Fig. S2. Phosphorylated PD-1 prefers Shp2 over Shp1.

(A) Rhodamine-PE (energy acceptor) bearing LUVs were reconstituted with purified Lck kinase and the cytosolic tail of PD-1, as shown in **Fig. 1A**. Full length phosphatase $Shp1^{FL}$ (left) or $Shp2^{FL}$ (middle) was purified as a SNAP-Tag fusion protein, labeled with SNAP-Cell-505 (energy acceptor), and presented in the extravesicular solution that contains 5 mM sodium orthovanadate to inhibit the phosphatase activities. Addition of ATP triggered Lck catalyzed phosphorylation of PD-1, which recruited the phosphatase to the LUV surface, leading to quenching of SNAP-Cell-505. Nine reactions containing increasing concentrations of PD-1 were run in parallel. The final extent of fluorescence quenching was plotted against PD-1 molecular density to determine the affinity of PD-1:$Shp2^{FL}$ or PD-1:$Shp1^{FL}$ interaction (right).

(B) A similar series of PD-1 titration FRET experiments were conducted with tandem SH2 domains of Shp1 ($Shp1^{tSH2}$) or Shp2 ($Shp1^{tSH2}$) that were labeled with SNAP-Cell-505. The final extent of fluorescence quenching was plotted against PD-1 densities (right). The apparent dissociation constant (K_d) were calculated by fitting the data with Graphpad Prism 5.0, using the "one site specific binding" model.

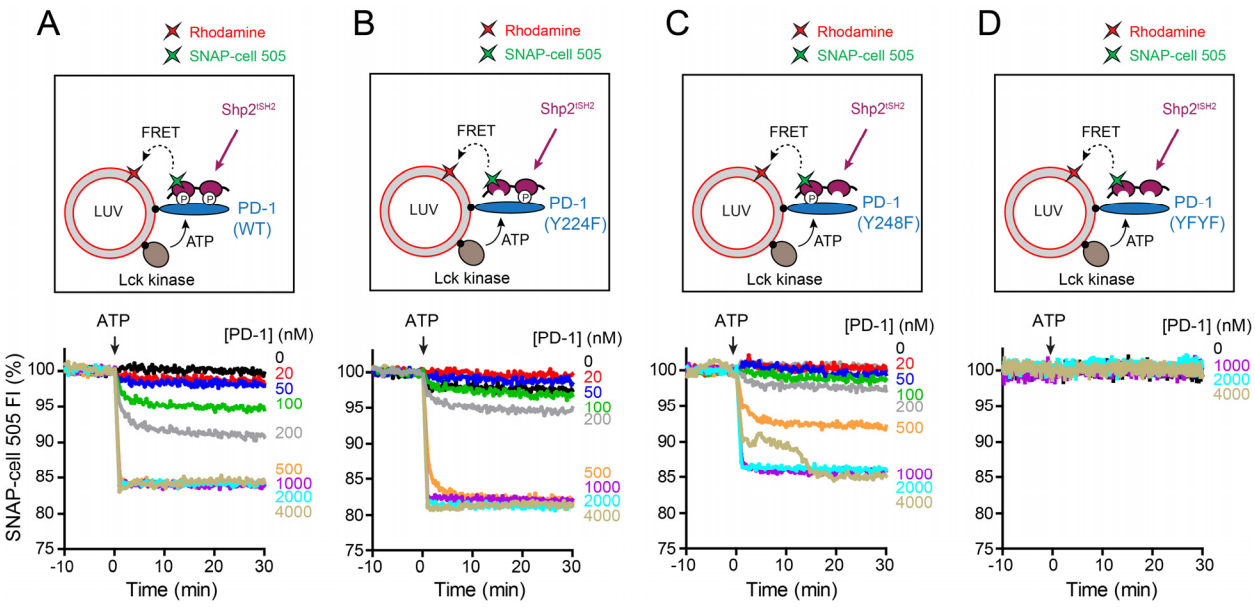

Fig. S3. The relative contributions of the two tyrosines of PD-1 in recruiting Shp2.

The FRET assay as shown in **Fig. 1A** was used to determine how tyrosine mutations affect the ability of PD-1 to recruit Shp2. The tandem SH2 domains of Shp2 ($Shp2^{tSH2}$) was purified as a SNAP-Tag fusion protein, labeled with SNAP-Cell-505 (energy acceptor), and presented in the extravesicular solution. Addition of ATP triggered Lck catalyzed phosphorylation of PD-1, which recruited certain SH2 proteins to the LUV surface, leading to quenching of the SNAP-Cell-505. To determine the affinity of PD-1-Shp2 interactions, nine reactions containing increasing concentrations of PD-1 were run in parallel. The final extent of fluorescence quenching was normalized and plotted against PD-1 concentrations, as shown in **Fig. 1C**. Four PD-1 variants were compared: WT PD-1 so that PD-1 can be doubly phosphorylated at both Y224 and Y248 by Lck **(panel A)**, PD-1 harboring an Y224F mutation so that PD-1 would become mono-phosphorylated at Y248 in response to ATP **(panel B)**, PD-1 harboring an Y248F mutation so that PD-1 would become mono-phosphorylated at Y224 in response to ATP **(panel C)**, and PD-1 with Y224F and Y248F mutations **(panel D)**.

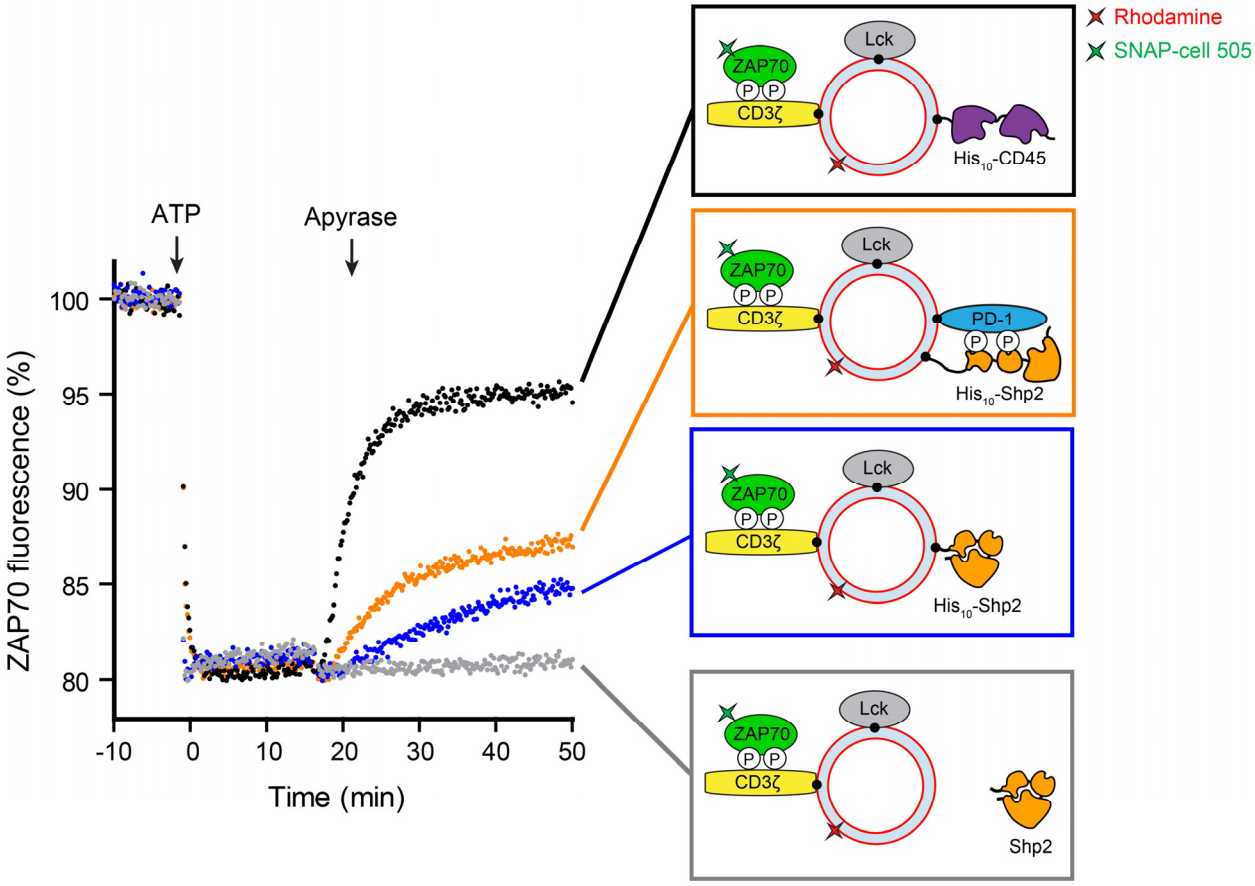

Fig. S4. PD-1 binding markedly upregulates Shp2 activity.

Membrane bound CD3ζ was utilized as a substrate to determine how PD-1 mediated membrane recruitment of Shp2 alters its tyrosine phosphatase activity. Recombinant His_{10} tagged CD3ζ and Lck were attached to LUVs containing DGS-NTA-Ni lipid and Rhodamine-PE. Three types of Shp2 were examined: (**i**) Shp2 presented in the extravesicular solution (grey); (**ii**) Shp2 tethered to the LUVs via an N-terminal His_{10}-tag (blue); (**iii**) Shp2 co-tethered to the LUVs with the cytosolic tail of PD-1 (orange). In the fourth condition, Shp2 was replaced with the cytosolic portion of CD45 tethered to the LUVs via a His_{10} tag (black). The tandem SH2 domains of ZAP70 was labeled with SNAP-Cell-505, and presented in the extravesicular solution as a fluorescence reporter for the phosphorylation state of CD3ζ. Addition of ATP triggers Lck mediated CD3ζ phosphorylation, led to membrane recruitment of ZAP70 and quenching of its fluorescence, due to energy transfer to Rhodamine-PE lipid, as reported previously (*40*). Note that in the presence of ATP, the kinase activity of Lck dominated over the phosphatase activity of Shp2 to cause net phosphorylation of CD3ζ. Subsequent addition of excess ATP scavenger apyrase rapidly inactivated Lck, and uncovered the phosphatase activity of Shp2 or CD45. Dephosphorylation of CD3ζ led to dissociation of ZAP70 and recovery of its fluorescence. Shown on the left are representative traces of ZAP70 fluorescence under all conditions. The initial slope of each fluorescence recovery trace was measured and used as an index for the relative phosphatase activity. Soluble Shp2 failed to recover ZAP70 fluorescence in response to apyrase (grey), indicating lack of phosphatase activity, in agreement with previous reports that Shp2 exists in an auto-inhibited form by itself (*53*); attaching Shp2 to LUVs strongly increased its phosphatase activity, causing appreciable recovery of ZAP70 fluorescence (blue), a result that is in parallel with our previous finding that membrane confinement promotes the kinase activity of Lck (*40*); co-attaching the cytosolic tail of PD-1 further accelerates the recovery of ZAP70 fluorescence (orange), suggesting that PD-1 binding "unlocked" the autoinhibited structure of Shp2, as reported for other phosphotyrosine containing peptides (*54*). CD45, an abundant phosphatase in T cells, exhibited much stronger phosphatase activity towards CD3ζ (black).

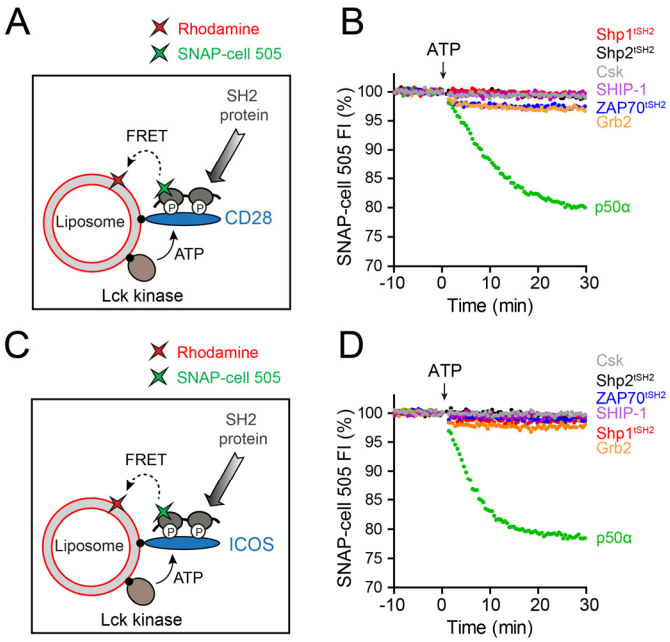

Fig. S5. Costimulatory receptors CD28 and ICOS both specifically recruit PI3K upon phosphorylation.

(**A**) Cartoon depicting a FRET assay for measuring the interaction between a SH2 containing protein and membrane bound cytosolic tail of CD28. Rhodamine-PE (energy acceptor) bearing LUVs were reconstituted with purified Lck kinase and the cytosolic domain of PD-1, as described in **Methods**. The SH2 proteins of interest was purified as a SNAP-Tag fusion protein, labeled with SNAP-Cell 505 (energy acceptor), and presented in the extravesicular solution. Addition of ATP triggered Lck catalyzed phosphorylation of CD28, which recruited certain SH2 proteins to the LUV surface, leading to FRET.

(**B**) A comparison of CD28 binding activities a panel of SH2 containing proteins, using the FRET assay as described in **A**. Shown are representative time courses of SNAP-Cell 505 fluorescence before and after the addition of ATP. Concentrations of components: 300 nM PD-1, 7.2 nM Lck and 100 nM labeled SH2 protein.

(**C, D**) Cartoon and representative traces of a FRET assay for measuring the interaction between a SH2 containing protein and membrane bound cytosolic tail of ICOS. Assay was identical to panel **A** except replacing CD28 with ICOS. p50α is the regulatory subunit of Type-I PI3K.

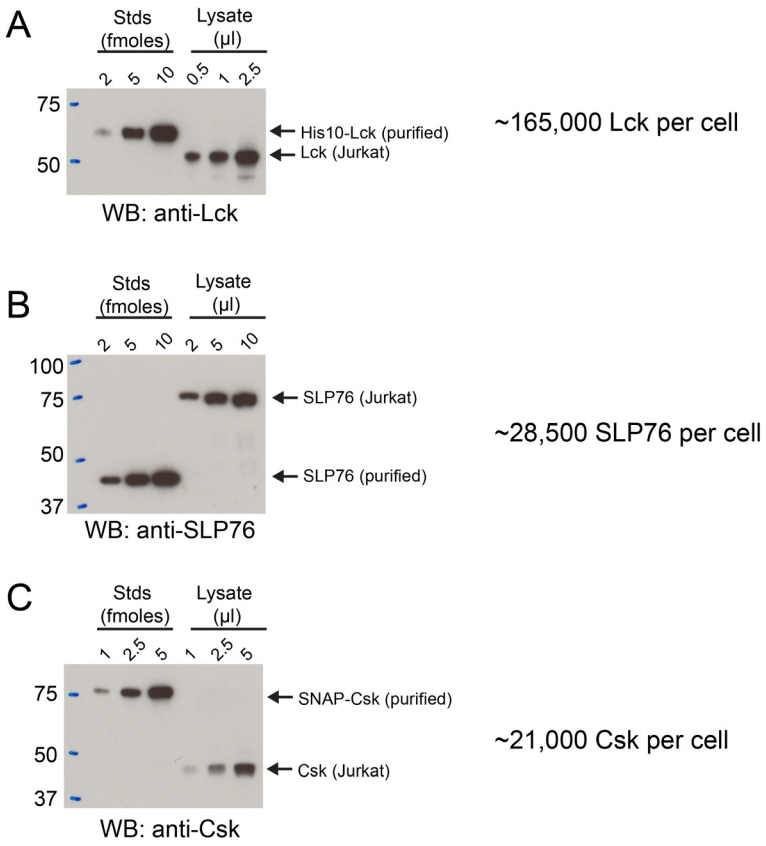

Fig. S6. Quantification of T cell signaling molecules using purified proteins as standards.

(**A-C**) Immunoblots showing indicated moles of purified protein standards and indicated volumes of Jurkat cell lysates side by side. Experiment was carried out as described in **Methods**. The optical densities of the bands were converted to protein mass, which were then used to calculate the copy numbers per cell, listed on the right.

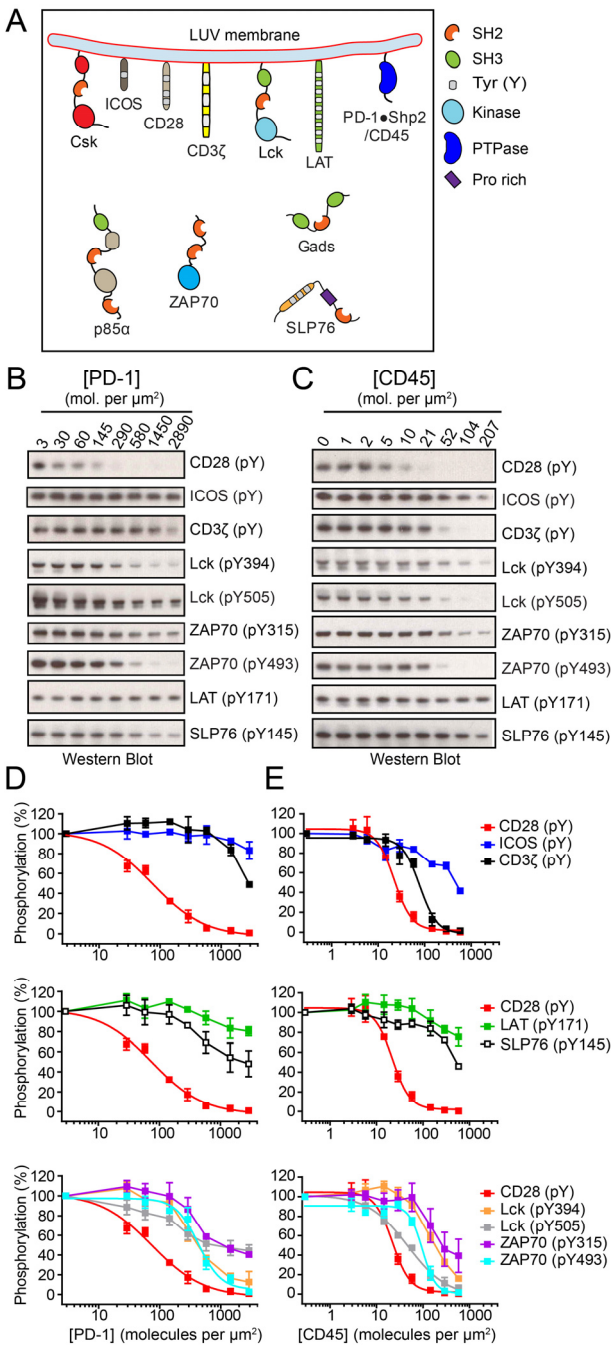

Fig. S7 PD-1 and CD45 dose responses in the presence of Csk.

(**A**) Cartoon depicting a LUV reconstitution system for assaying the sensitivities of different targets to PD-1•Shp2 or to CD45, same as shown in **Fig. 2A** except in the presence of membrane bound Csk.

(**B, C**) Phosphotyrosine Western blots for a subset of TCR and costimulatory receptors (CD28 and ICOS) as a function of PD-1 or CD45 concentration. Titration was conducted as described in **Fig. 2A, B** except in the presence of 50 nM His_{10}-Csk (or ~145 molecules per μm^2).

(**D, E**) The optical density of each band in **B, C** was quantified by ImageJ and plotted against PD-1 or CD45 molecular densities. *Upper panel*, dose responses for receptors. *Middle panel*, dose responses for adaptors LAT and SLP76. *Lower panel*, PD-1 dose responses for tyrosine kinases Lck and ZAP70. The CD28 dose response curve as shown in each panel for comparison. All dose response data were fit using Graphpad Prism 5.0, and IC_{50} values expressed in molecules per μm^2 and summarized in **Table S2**. Error bars: S.D., $n = 3$ independent experiments.

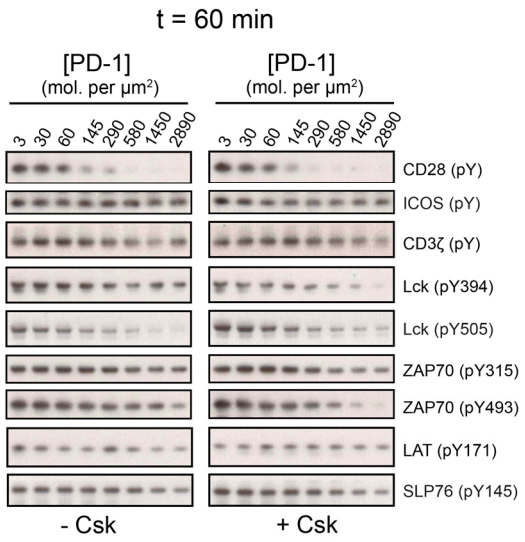

Fig. S8 CD28 remained the most sensitive to PD-1 bound Shp2 at a later time point.

The same PD-1 titration experiments as in **Fig. 2** except terminated at a later time point: 60 min after the addition of ATP.

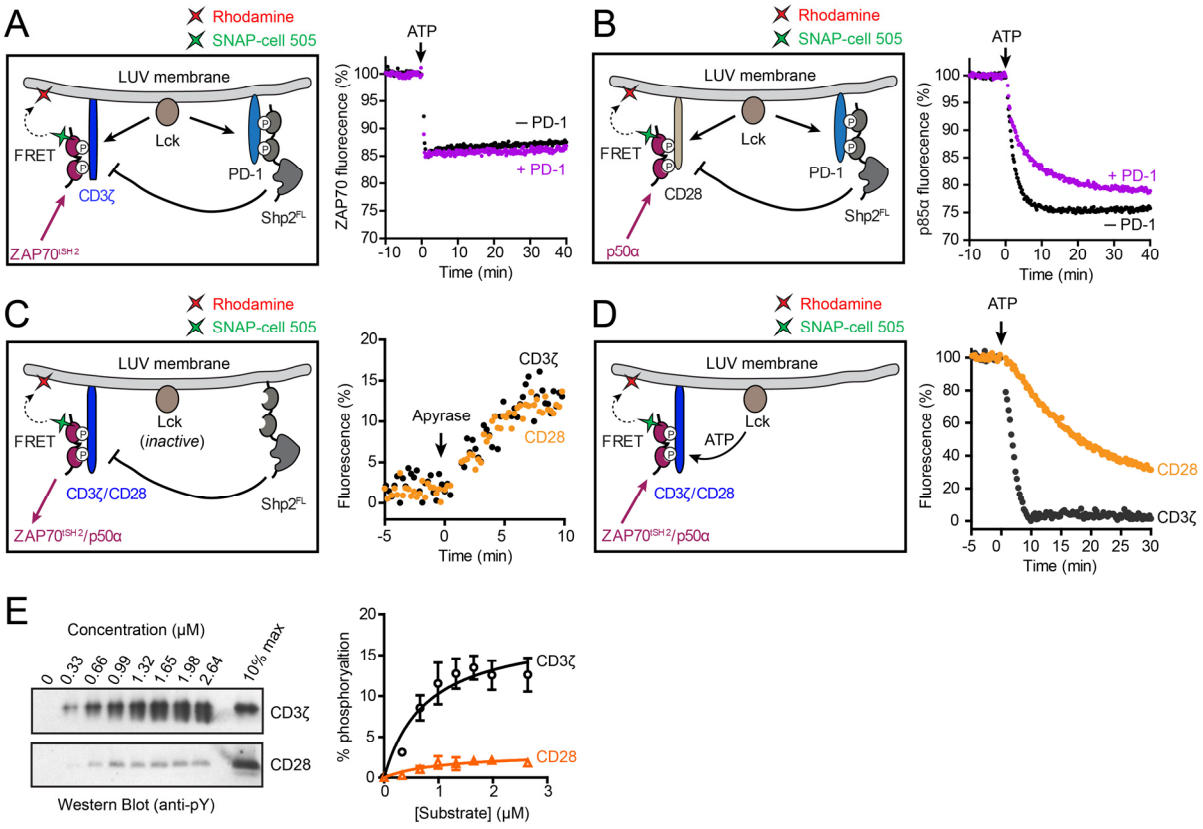

Fig. S9 Mechanism of CD28 preference of PD-1: a weaker kinase activity.
(**A**) A liposome reconstitution assay for measuring the PD-1 effect on TCR phosphorylation, in the absence of costimulatory receptors. The cytosolic domains of CD3ζ, PD-1 and Lck were tethered onto Rhodamine-PE (FRET acceptor) containing, DGS-NTA-Ni liposomes via an N-terminal His_{10}-tag, as described in **Methods**. $ZAP70^{tSH2}$was labeled with SNAP-Cell 505 (FRET acceptor) and presented in the extravesicular solution. The purple trace shows the time course of SNAP-Cell 505 fluorescence before and after the addition of ATP. The black trace shows a parallel experiment in the absence of PD-1.

(**B**) A liposome reconstitution assay for measuring the PD-1 effect on CD28 phosphorylation, in the absence of TCR. Experiment was identical to *panel A* except replacing CD3ζ with CD28, and replacing $ZAP70^{tSH2}$ with the regulatory subunit of PI3K (p50α).

(**C**) A liposome reconstitution assay for comparing the Shp2 phosphatase activity towards CD28 and CD3ζ. His_{10}-Shp2 and excess His_{10}-Lck was co-attached onto Rhodamine-PE containing liposomes with either His_{10}-CD3ζ or His_{10}-CD28, and $ZAP70^{tSH2}$*505 or p50α*505 was used as a reporter to probe the phosphorylation state of CD3ζ or CD28, respectively. ATP was added first, allowing Lck to phosphorylate CD3ζ or CD28, bringing either $ZAP70^{tSH2}$*505 or p50α*505 to the membranes (data not shown). Subsequent addition of the ATP scavenger apyrase terminated the kinase activity, allowing the Shp2 catalyzed dephosphorylation of either CD3ζ or CD28, reflected by de-quenching of the FRET donor SNAP-Cell 505.

(**D**) A liposome reconstitution assay for comparing the Lck kinase activity towards CD28 and CD3ζ. His_{10}-Lck was co-attached onto Rhodamine-PE containing liposomes with either His_{10}-CD3ζ or His_{10}-CD28, and $ZAP70^{tSH2}$*505 or p50α*505 was used as a reporter to probe the phosphorylation state of CD3ζ or CD28, respectively. Shown in black and red are the time courses of ZAP70 recruitment to CD3ζ, and PI3K recruitment to CD28 respectively.

(**E**) Michaels–Menton kinetics of Lck catalyzed CD3ζ or CD28 phosphorylation. (*Left*) Western blot of CD3ζ or CD28 phosphorylation (1 min) by Lck at indicated concentrations of substrate. The rightmost lane was loaded with 10% of maximally phosphorylated substrate at its highest concentration (2.64 μM), achieved by letting the kinase reaction run into completion (60 min). (*Right*) The 5 min signals, quantified with ImageJ, were normalized to the maximum phosphorylation signal (80 min), plotted against substrate (CD3ζ or CD28) concentration, and fit with Michaelis–Mention equation using Graphpad Prism 5.0 (see **Methods**). Error bars: S.D., $n = 3$ independent experiments.

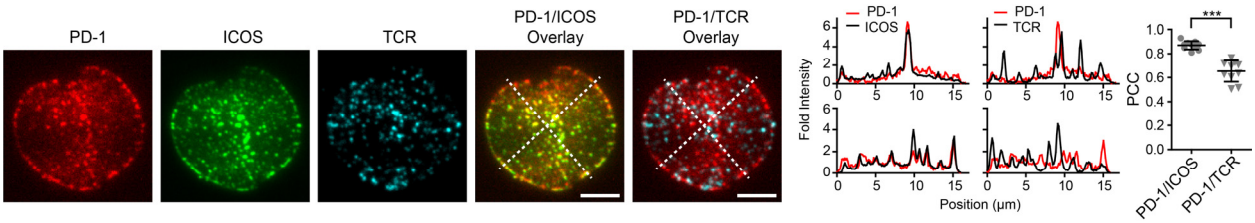

Fig. S10. PD-1 coclusters with costimulatory receptor ICOS.

(*Left*) Representative TIRF images of PD-1, ICOS and TCR of an OT-I CD8+ T cell 10 sec after landing onto a lipid bilayer functionalized with recombinant ligands (100 – 250 molecules per μm^2), which included peptide-loaded MHC-I (H2Kb), ICOSL (ICOS ligand), and ICAM-1 (integrin LFA1 ligand). Cells were retrovirally transduced with PD-1–mCherry and ICOS–mGFP and TCR was labeled with an Alexa Fluor647 conjugated anti-TCR antibody (see **Methods)**. Scale bars: 5 μm. (*Middle*) Intensities were calculated from the raw fluorescence intensities along the two diagonal lines in the overlaid images (see **Methods**). PD-1: red; ICOS or TCR: black. (*Right*) Column scattered plot summarizing the Pearson's correlation coefficient (PCC) values for PD-1/ICOS overlay (0.87 ± 0.04, mean ± S.D) and for PD-1/TCR overlay (0.65 ± 0.03) of 10 fully spread cells from three independent experiments, with each dot representing a unique cell. Statistical significance was evaluated by two-tailed Student's t test, $P < 0.0001$.

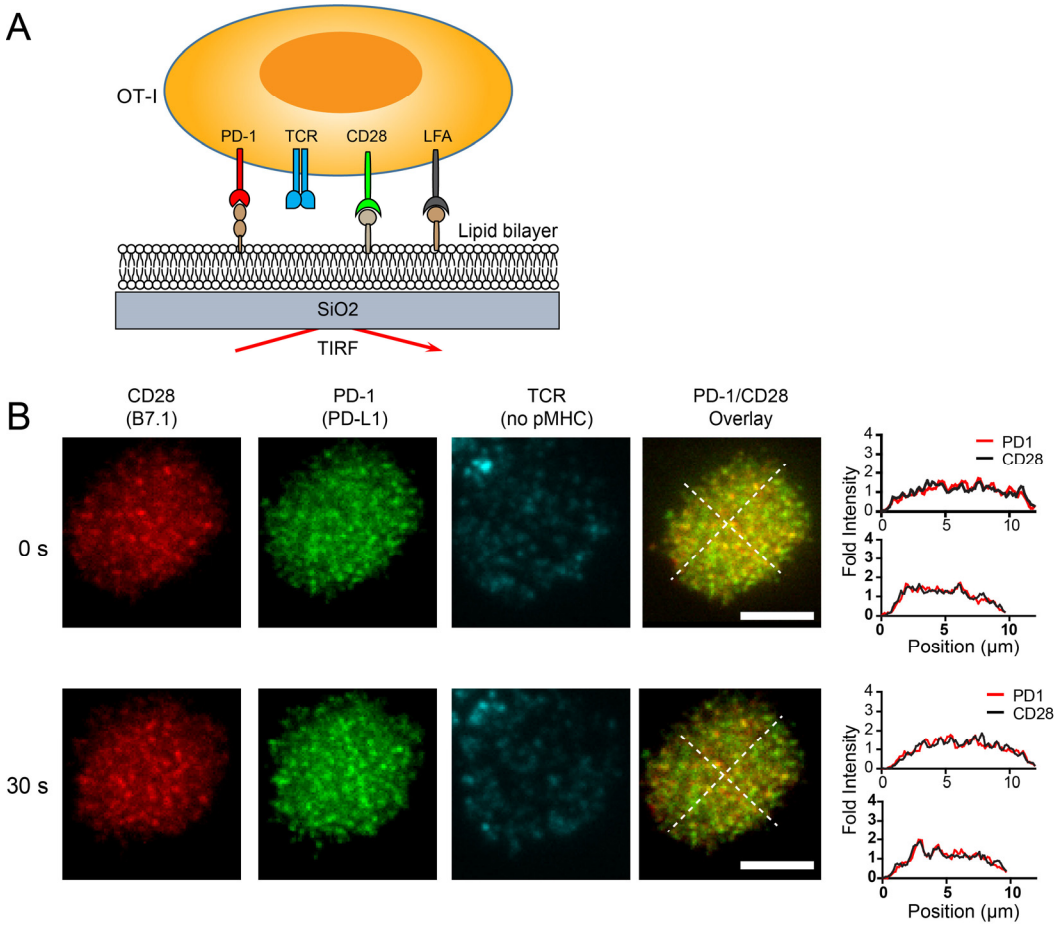

Fig. S11. PD-1 microclusters depend on the presence of PD-L1 on the bilayer.

(**A**) A supported lipid bilayer system for visualizing receptor localization at the immunological synapse. The bilayer was functionalized as in **Fig. 3** except without H2Kb-SIINFEKL.

(**B**) Representative TIRF microscopy images of PD-1, CD28 and TCR of a PD-1–mCherry and CD28–mGFP expressing OT-I cell 0 second and 10 seconds after the bilayer contact. The PD-1 and CD28 images were overlaid and line scan analyses were presented as fold intensity histograms. Scale bars: 5 μm.

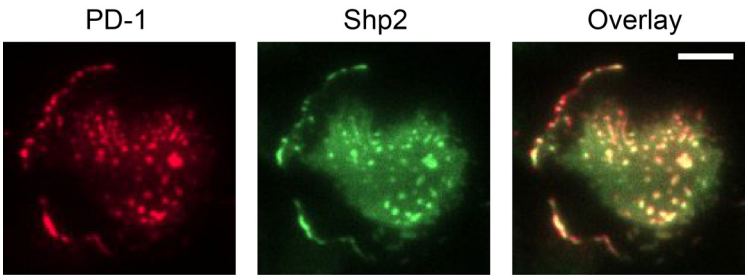

Fig. S12. The protein tyrosine phosphatase Shp2 is recruited to PD-1 microclusters.

Representative TIRF microscopy images of an OT-I cell co-transduced with PD-1–mCherry and Shp2–mGFP, 20 seconds after landing to a bilayer that was functionalized with H2Kb-SIINFEKL and PD-L1. Scale bar: 5 μm.

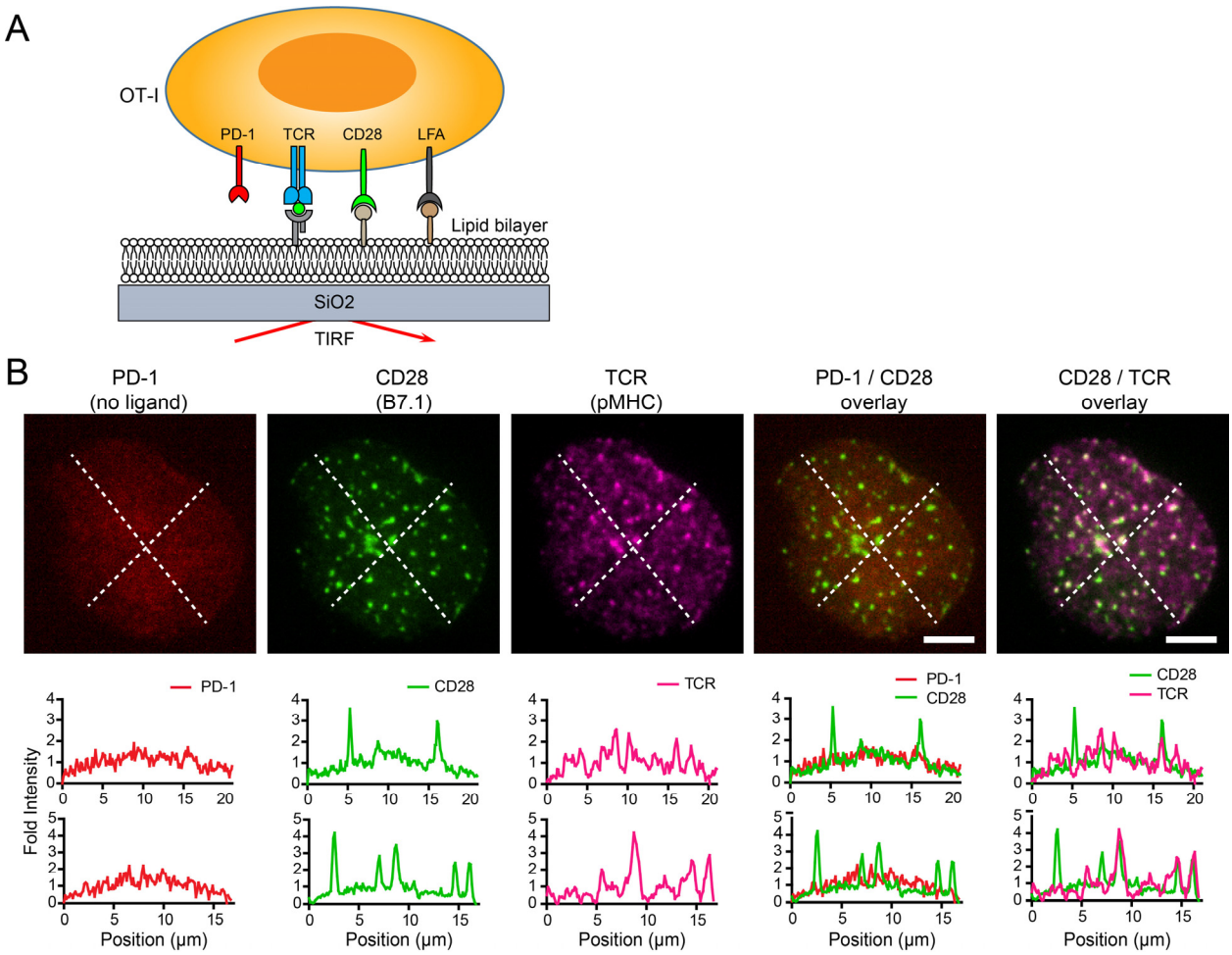

Fig. S13. PD-1 microclusters depend on the presence of PD-L1 on the bilayer.

(**A**) A supported lipid bilayer system for visualizing receptor localization at the immunological synapse. The bilayer was functionalized as in **Fig. 3** except without PD-L1.

(**B**) Representative TIRF images of PD-1, CD28 and TCR of an OT-I cell 10 seconds after the bilayer contact. The OT-I cells were retrovirally transduced with PD-1–mCherry and CD28–mGFP, and the TCR was labeled with Alexa Fluor647 conjugated single chain variable fragment of the H57-597 anti-TCRβ antibody, as described in the **Methods.** Shown on the right are overlaid images for PD-1/CD28 and CD28/TCR. Scale bars: 5 μm.

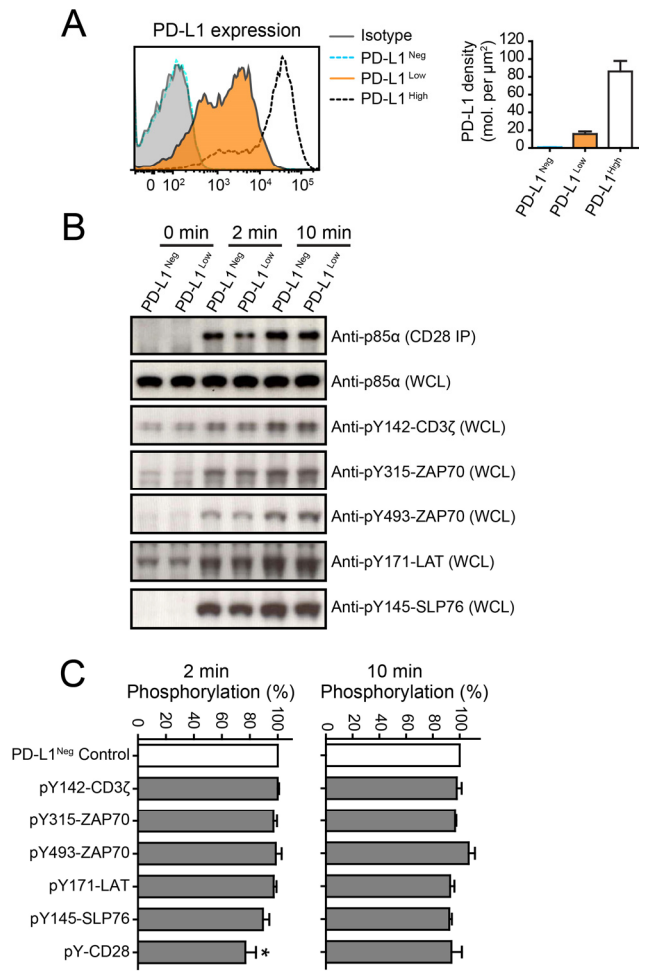

Fig. S14. Low strength of PD-L1–PD-1 signaling selectively suppress CD28 signaling.

(**A**) (*Left*) FACS histograms highlighting Raji B cells that express intermediate levels of PD-L1 ($PDL1^{Low}$, orange trace), in comparison with PD-L1 negative parental Raji ($PD\text{-}L1^{-}$, green dashed trace) and $PD\text{-}L1^{High}$ Raji (black dash trace). (*Right*) Bar graph summarizing the PD-L1 densities in $PD\text{-}L1^{-}$, $PD\text{-}L1^{Low}$ and $PD\text{-}L1^{High}$ Raji, as quantified by BD Quantibrite kit (**Methods**).

(**B**) Western blots showing that low levels of PD-L1 on antigen loaded Raji B cells modulated CD28 and TCR signaling components in Jurkat T cells. Experiments were conducted as in **Fig. 4** except using either 100% of $PD\text{-}L1^{Low}$ Raji or 100% of $PD\text{-}L1^{-}$ Raji as APCs. (**C**) Bar graphs summarizing 2 min and 10 min data in panel **B**, in which the phosphorylation signals under $PD\text{-}L1^{Low}$ conditions were normalized to $PD\text{-}L1^{-}$ conditions**.** Error bars: standard deviations (n = 3 independent experiments).

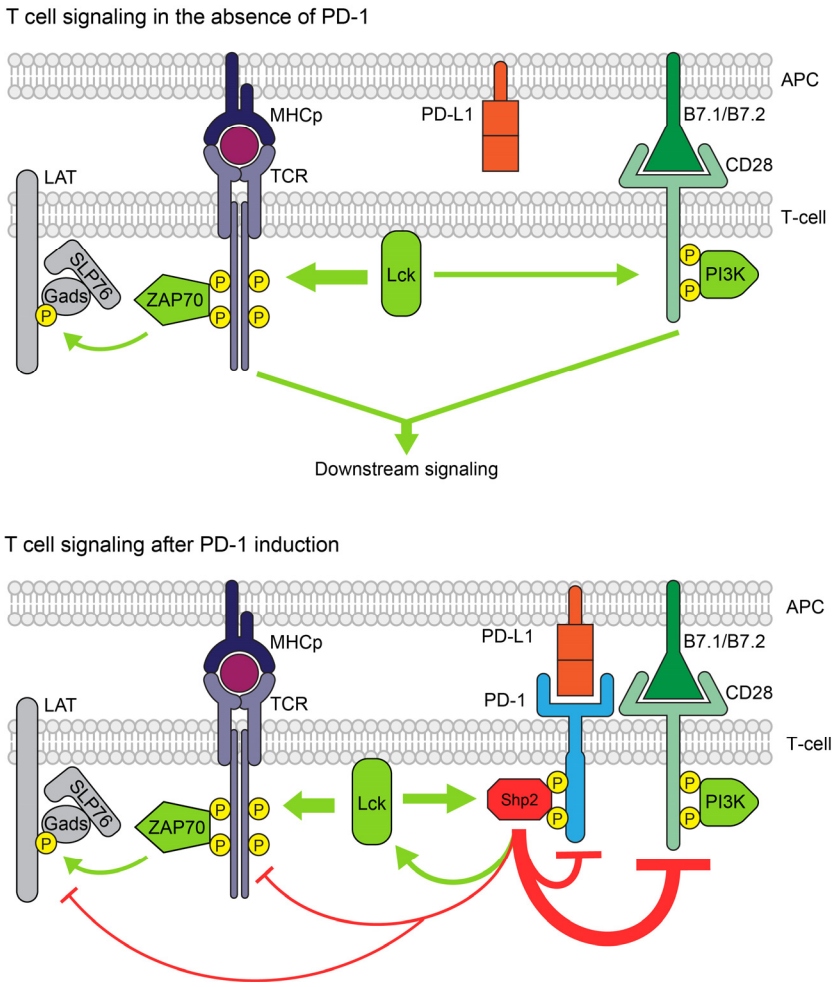

Fig. S15 Working model for how PD-1 suppresses T cell signaling.

(**A**) In naïve T cells, PD-1 is expressed at very low levels. Engagement of TCR and the costimulatory receptor CD28 on the T cell with their respective ligands on the APC triggers Lck catalyzed tyrosine phosphorylation of their cytosolic tails, which recruits ZAP70 and PI3K (**fig. S5**) to the plasma membrane. ZAP70 and PI3K then catalyze multiple phosphorylation reactions to collectively activate T cells.

(**B**) In an activated or an "exhausted" T cell, PD-1 becomes expressed. Engagement of PD-1 with its ligand PD-L1 on APCs triggers the phosphorylation of two tyrosines contained at the PD-1 cytosolic tail. Phosphorylated PD-1 specifically recruits the protein tyrosine phosphatase Shp2 to the plasma membrane (**Fig. 1B** and **fig. S2A**). The otherwise auto-inhibited Shp2 become strongly activated after binding to phosphorylated PD-1 (**fig. S4**), and preferentially dephosphorylates the cytosolic tail of the costimulatory receptor CD28 to suppress T cell activation. In contrast, the TCR and its downstream components are more resistant to PD-1 mediated inhibition (**Fig. 2, Fig. 4** and **fig. S14**). The PD-1–Shp2 complex is highly unstable due to the ability of Shp2 to dephosphorylate PD-1 (**Fig. 1G, H**). This biochemical instability might underlie the transient PD-1 mediated dephosphorylation at the receptor level (**Fig. 4C, D**).

Table S1. Physiological levels of T cell signaling proteins

Membrane protein	Copies per cell	References	Cell type	Molecules per μm² in cells	Molecules per μm² in Fig. 2
TCR	12,000	A. Weiss, personal communication	Jurkat T cells	29	290
	15,000 - 20,000	Reference (*55*)	human T cells	150 - 200	
	100,000	Reference (*56*)	2C transgenic cytotoxic T cells	1020	
Lck	608,000	Reference (*57*)	Jurkat T cells	1460	290
	58,000	Reference (*57*)	mouse CD4+ T cells	590	
	78,000	Reference (*57*)	mouse CD8+ T cells	790	
	165,000	Western Blot, **fig. S6**	Jurkat T cells	390	
CD28	60,000	Reference (*58*)	human primary T cells	610	870
	22,800 ± 4,000	BD Quantibrite kit	Jurkat T cells	55	
	4,720 ± 1230	BD Quantibrite kit	mouse CD8+ T cells	48	
ICOS	N/A	N/A	N/A	N/A	870
LAT	370,000	Reference (*59*)	Jurkat T cells	890	870
PD-1	20,000 - 100,000	Reference (*60*)	Anti-CD3/anti-CD28/IL2 stimulated primary T cells	200 - 1000	0 - 2800
	43 ± 2	BD Quantibrite kit	Naïve CD4+ T cells	0	
	1,230 ± 21	BD Quantibrite kit	Antibodies stimulated CD4+ T cells	12	
	516 ± 97	BD Quantibrite kit	CT26 tumor infiltrating CD4+ T cells	5.2	
	162 ± 27	BD Quantibrite kit	LCMV CD4+ T cells	1.6	
	24 ± 1	BD Quantibrite kit	Naïve CD8+ T cells	0.2	
	671 ± 16	BD Quantibrite kit	Antibodies stimulated CD8+ T cells	6.8	
	300 ± 61	BD Quantibrite kit	LCMV CD8+ T cells	3.0	
	1,084 ± 686	BD Quantibrite kit	CT26 tumor infiltrating CD8+ T cells	11	
	1,341 ± 101	BD Quantibrite kit	PD-1 transduced OT-I CD8+ T cells	14	
	430 ± 41	BD Quantibrite kit	Jurkat T cells	1	
	16,543 ± 2,250	BD Quantibrite kit	PD-1 transfected Jurkat T cells	40	
Cytosolic protein	**Copies per cell**	**References**	**Cell type**	**Cytosolic concentration**	**Molar concentration in Fig. 2**
ZAP70	515,000*	maxQB database, Reference (*61*)	Jurkat T cells	1 μM	0.3 μM
	50,000	A. Weiss, personal communication	Jurkat T cells	0.1 μM	
Shp2	126,000*	maxQB database, Reference (*61*)	Jurkat T cells	0.3 μM	0.3 μM
p85α	18,000*	maxQB database, Reference (*61*)	Jurkat T cells	0.04 μM	0.2 μM**
GADS	449,000*	maxQB database, Reference (*61*)	Jurkat T cells	0.9 μM	0.3 μM
SLP76	29,000	Western Blot, **fig. S6**	Jurkat T cells	0.06 μM	0.3 μM

Csk	21,000	Western Blot, **fig. S6**	Jurkat T cells	0.04 μM	0.05 μM

Table S1. Physiological levels of T cell signaling proteins. Molecular density on the cell membrane was estimated by dividing the copy number with the surface area, assuming non-convoluted plasma membrane, 11.5 μm diameter for Jurkat T cells (*62*) and 5.6 μm diameter for primary T cells (*63*).

*These copy numbers were calculated based on the iBAQ values deposited in the maxQB database, assuming 20,000 copies of TCR per cell (*55*), or 40,000 copies of CD3ζ per cell.

**0.2 μM were used here to account for the five splice variants of PI3K regulatory subunits (*64*).

Table S2. Summary of IC50 values for PD-1 and CD45 dose responses

	IC_{50} for PD-1 (molecules per μm^2)		IC_{50} for CD45 (molecules per μm^2)	
Target	- Csk	+ Csk	- Csk	+ Csk
CD28 (pY)	96	75	24	22
ICOS (pY)	> 3000	> 3000	300 - 600	300 - 600
CD3ζ (pY)	> 3000	~3000	94	78
Lck (Y394)	~600	~300	300 - 600	150 - 300
Lck (Y505)	400	~600	32	47
ZAP70 (Y315)	~3000	600 - 1500	150 - 300	150 - 300
ZAP70 (Y493)	~1400	430	85	89
LAT (pY171)	> 3000	> 3000	150 - 300	> 1000
SLP76 (pY145)	~ 3000	> 3000	300 - 600	300 - 600

Table S2. Summary of 50% inhibition concentrations (IC_{50}) for PD-1 and CD45 dose responses. These values were calculated based on data presented in **Fig. 2** (without membrane bound Csk, denoted as "- Csk") and **fig. S7** (with membrane bound Csk, denoted as "+ Csk"), as described in Methods.

Table S3. PD-L1 expression levels under physiological contexts and in transfected cells

Membrane protein	Copies per cell	Method	Cell type	Molecules per μm^2 on cell membrane
PD-L1	3860 ± 1450	BD Quantibrite kit	MC38 tumor infiltrating CD11b+ Ly6G- Ly6C- F4/80+ macrophages	3.1
	790 ± 490	BD Quantibrite kit	MC38 tumor infiltrating monocytic myeloid-derived suppressor cells (mo-MDSCs)	2.5
	790 ± 490	BD Quantibrite kit	MC38 tumor infiltrating granulocytic myeloid-derived suppressor cells (g-MDSCs)	2.5
	140 ± 20	BD Quantibrite kit	MC38 tumor infiltrating CD8+ T cells	1.4
	470 ± 40	BD Quantibrite kit	MC38 tumor infiltrating CD4+ T cells	4.8
	1600 ± 310	BD Quantibrite kit	MC38 CD45- tumor cells	2.2
	900 ± 30	BD Quantibrite kit	MC38 spleen derived CD11b+ Ly6G- Ly6C- F4/80+ Macrophages	0.7
	40 ± 3	BD Quantibrite kit	MC38 spleen derived monocytes	0.1
	120 ± 20	BD Quantibrite kit	MC38 spleen derived neurophils	0.4
	250 ± 30	BD Quantibrite kit	MC38 spleen derived CD8+ T cells	2.5
	240 ± 30	BD Quantibrite kit	MC38 spleen derived CD4+ T cells	2.4
	300 ± 30	BD Quantibrite kit	Parental Raji B cells	0.1
	6500 ± 840	BD Quantibrite kit	PD-L1^{Low} Raji B cells	12
	35800 ± 3500	BD Quantibrite kit	PD-L1^{High} Raji B cells	68

Table S3. PD-L1 expression levels under physiological contexts and in transfected cells. Molecular density on the cell membrane was estimated by dividing the copy number with the surface area, assuming non-convoluted plasma membranes. Diameter values used for estimating PD-L1 densities: 20 µm for macrophages, 10 µm for MDSCs and neutrophils, 5.6 µm for T cells, 15.2 µm for tumor cells, 12 µm for monocytes, and 13 µm for Raji B cells.

Supplementary Movie Legends

Movie S1.
A TIRF microscopy time-lapse video of the representative OT-I cell co-expressing mouse PD-1–mCherry, mouse CD28–mGFP after bilayer contact, as shown in **Fig. 3A**. PD-1, CD28 and TCR were rendered in red, green and cyan, respectively, using Fiji. Interval: 5 sec.

Movie S2.
A TIRF microscopy time-lapse video of the representative OT-I cell co-expressing mouse PD-1–mCherry, mouse CD28–mGFP after contacting a bilayer that contains pMHC, LFA and B7.1, but lacks PD-L1, as shown in **fig. S13**. PD-1, CD28 and TCR were rendered in red, green and cyan, respectively, using Fiji. Interval: 5 sec.

References and Notes

1. L. Chen, D. B. Flies, Molecular mechanisms of T cell co-stimulation and co-inhibition. *Nat. Rev. Immunol.* **13**, 227–242 (2013). doi:10.1038/nri3405 Medline

2. D. S. Chen, I. Mellman, Oncology meets immunology: The cancer-immunity cycle. *Immunity* **39**, 1–10 (2013). doi:10.1016/j.immuni.2013.07.012 Medline

3. M. E. Keir, M. J. Butte, G. J. Freeman, A. H. Sharpe, PD-1 and its ligands in tolerance and immunity. *Annu. Rev. Immunol.* **26**, 677–704 (2008). doi:10.1146/annurev.immunol.26.021607.090331 Medline

4. G. J. Freeman, A. J. Long, Y. Iwai, K. Bourque, T. Chernova, H. Nishimura, L. J. Fitz, N. Malenkovich, T. Okazaki, M. C. Byrne, H. F. Horton, L. Fouser, L. Carter, V. Ling, M. R. Bowman, B. M. Carreno, M. Collins, C. R. Wood, T. Honjo, Engagement of the PD-1 immunoinhibitory receptor by a novel B7 family member leads to negative regulation of lymphocyte activation. *J. Exp. Med.* **192**, 1027–1034 (2000). doi:10.1084/jem.192.7.1027 Medline

5. H. Dong, S. E. Strome, D. R. Salomao, H. Tamura, F. Hirano, D. B. Flies, P. C. Roche, J. Lu, G. Zhu, K. Tamada, V. A. Lennon, E. Celis, L. Chen, Tumor-associated B7-H1 promotes T-cell apoptosis: A potential mechanism of immune evasion. *Nat. Med.* **8**, 793–800 (2002). doi:10.1038/nm0902-1039c Medline

6. J. M. Taube, R. A. Anders, G. D. Young, H. Xu, R. Sharma, T. L. McMiller, S. Chen, A. P. Klein, D. M. Pardoll, S. L. Topalian, L. Chen, Colocalization of inflammatory response with B7-H1 expression in human melanocytic lesions supports an adaptive resistance mechanism of immune escape. *Sci. Transl. Med.* **4**, 127ra37 (2012). doi:10.1126/scitranslmed.3003689 Medline

7. E. J. Wherry, M. Kurachi, Molecular and cellular insights into T cell exhaustion. *Nat. Rev. Immunol.* **15**, 486–499 (2015). doi:10.1038/nri3862 Medline

8. C. L. Day, D. E. Kaufmann, P. Kiepiela, J. A. Brown, E. S. Moodley, S. Reddy, E. W. Mackey, J. D. Miller, A. J. Leslie, C. DePierres, Z. Mncube, J. Duraiswamy, B. Zhu, Q. Eichbaum, M. Altfeld, E. J. Wherry, H. M. Coovadia, P. J. R. Goulder, P. Klenerman, R. Ahmed, G. J. Freeman, B. D. Walker, PD-1 expression on HIV-specific T cells is associated with T-cell exhaustion and disease progression. *Nature* **443**, 350–354 (2006). doi:10.1038/nature05115 Medline

9. M. J. Butte, M. E. Keir, T. B. Phamduy, A. H. Sharpe, G. J. Freeman, Programmed death-1 ligand 1 interacts specifically with the B7-1 costimulatory molecule to inhibit T cell responses. *Immunity* **27**, 111–122 (2007). doi:10.1016/j.immuni.2007.05.016 Medline

10. L. Baitsch, P. Baumgaertner, E. Devêvre, S. K. Raghav, A. Legat, L. Barba, S. Wieckowski, H. Bouzourene, B. Deplancke, P. Romero, N. Rufer, D. E. Speiser, Exhaustion of tumor-specific $CD8^+$ T cells in metastases from melanoma patients. *J. Clin. Invest.* **121**, 2350–2360 (2011). doi:10.1172/JCI46102 Medline

11. P. Sharma, J. P. Allison, The future of immune checkpoint therapy. *Science* **348**, 56–61 (2015). doi:10.1126/science.aaa8172 Medline

12. D. M. Pardoll, The blockade of immune checkpoints in cancer immunotherapy. *Nat. Rev. Cancer* **12**, 252–264 (2012). doi:10.1038/nrc3239 Medline

13. I. Mellman, G. Coukos, G. Dranoff, Cancer immunotherapy comes of age. *Nature* **480**, 480–489 (2011). doi:10.1038/nature10673 Medline

14. K. E. Pauken, E. J. Wherry, Overcoming T cell exhaustion in infection and cancer. *Trends Immunol.* **36**, 265–276 (2015). doi:10.1016/j.it.2015.02.008 Medline

15. R. S. Herbst, J.-C. Soria, M. Kowanetz, G. D. Fine, O. Hamid, M. S. Gordon, J. A. Sosman, D. F. McDermott, J. D. Powderly, S. N. Gettinger, H. E. K. Kohrt, L. Horn, D. P. Lawrence, S. Rost, M. Leabman, Y. Xiao, A. Mokatrin, H. Koeppen, P. S. Hegde, I. Mellman, D. S. Chen, F. S. Hodi, Predictive correlates of response to the anti-PD-L1 antibody MPDL3280A in cancer patients. *Nature* **515**, 563–567 (2014). doi:10.1038/nature14011 Medline

16. T. Powles, J. P. Eder, G. D. Fine, F. S. Braiteh, Y. Loriot, C. Cruz, J. Bellmunt, H. A. Burris, D. P. Petrylak, S. L. Teng, X. Shen, Z. Boyd, P. S. Hegde, D. S. Chen, N. J. Vogelzang, MPDL3280A (anti-PD-L1) treatment leads to clinical activity in metastatic bladder cancer. *Nature* **515**, 558–562 (2014). doi:10.1038/nature13904 Medline

17. N. A. Rizvi, J. Mazières, D. Planchard, T. E. Stinchcombe, G. K. Dy, S. J. Antonia, L. Horn, H. Lena, E. Minenza, B. Mennecier, G. A. Otterson, L. T. Campos, D. R. Gandara, B. P. Levy, S. G. Nair, G. Zalcman, J. Wolf, P.-J. Souquet, E. Baldini, F. Cappuzzo, C. Chouaid, A. Dowlati, R. Sanborn, A. Lopez-Chavez, C. Grohe, R. M. Huber, C. T. Harbison, C. Baudelet, B. J. Lestini, S. S. Ramalingam, Activity and safety of nivolumab, an anti-PD-1 immune checkpoint inhibitor, for patients with advanced, refractory squamous non-small-cell lung cancer (CheckMate 063): A phase 2, single-arm trial. *Lancet Oncol.* **16**, 257–265 (2015). doi:10.1016/S1470-2045(15)70054-9 Medline

18. O. Hamid, C. Robert, A. Daud, F. S. Hodi, W.-J. Hwu, R. Kefford, J. D. Wolchok, P. Hersey, R. W. Joseph, J. S. Weber, R. Dronca, T. C. Gangadhar, A. Patnaik, H. Zarour, A. M. Joshua, K. Gergich, J. Elassaiss-Schaap, A. Algazi, C. Mateus, P. Boasberg, P. C. Tumeh, B. Chmielowski, S. W. Ebbinghaus, X. N. Li, S. P. Kang, A. Ribas, Safety and tumor responses with lambrolizumab (anti-PD-1) in melanoma. *N. Engl. J. Med.* **369**, 134–144 (2013). doi:10.1056/NEJMoa1305133 Medline

19. S. L. Topalian, F. S. Hodi, J. R. Brahmer, S. N. Gettinger, D. C. Smith, D. F. McDermott, J. D. Powderly, R. D. Carvajal, J. A. Sosman, M. B. Atkins, P. D. Leming, D. R. Spigel, S. J. Antonia, L. Horn, C. G. Drake, D. M. Pardoll, L. Chen, W. H. Sharfman, R. A. Anders, J. M. Taube, T. L. McMiller, H. Xu, A. J. Korman, M. Jure-Kunkel, S. Agrawal, D. McDonald, G. D. Kollia, A. Gupta, J. M. Wigginton, M. Sznol, Safety, activity, and immune correlates of anti-PD-1 antibody in cancer. *N. Engl. J. Med.* **366**, 2443–2454 (2012). doi:10.1056/NEJMoa1200690 Medline

20. K. A. Sheppard, L. J. Fitz, J. M. Lee, C. Benander, J. A. George, J. Wooters, Y. Qiu, J. M. Jussif, L. L. Carter, C. R. Wood, D. Chaudhary, PD-1 inhibits T-cell receptor induced phosphorylation of the ZAP70/CD3ζ signalosome and downstream signaling to PKCθ. *FEBS Lett.* **574**, 37–41 (2004). doi:10.1016/j.febslet.2004.07.083 Medline

21. T. Yokosuka, M. Takamatsu, W. Kobayashi-Imanishi, A. Hashimoto-Tane, M. Azuma, T. Saito, Programmed cell death 1 forms negative costimulatory microclusters that directly

inhibit T cell receptor signaling by recruiting phosphatase SHP2. *J. Exp. Med.* **209**, 1201–1217 (2012). doi:10.1084/jem.20112741 Medline

22. J. Zikherman, C. Jenne, S. Watson, K. Doan, W. Raschke, C. C. Goodnow, A. Weiss, CD45-Csk phosphatase-kinase titration uncouples basal and inducible T cell receptor signaling during thymic development. *Immunity* **32**, 342–354 (2010). doi:10.1016/j.immuni.2010.03.006 Medline

23. B. H. Zinselmeyer, S. Heydari, C. Sacristán, D. Nayak, M. Cammer, J. Herz, X. Cheng, S. J. Davis, M. L. Dustin, D. B. McGavern, PD-1 promotes immune exhaustion by inducing antiviral T cell motility paralysis. *J. Exp. Med.* **210**, 757–774 (2013). doi:10.1084/jem.20121416 Medline

24. R. V. Parry, J. M. Chemnitz, K. A. Frauwirth, A. R. Lanfranco, I. Braunstein, S. V. Kobayashi, P. S. Linsley, C. B. Thompson, J. L. Riley, CTLA-4 and PD-1 receptors inhibit T-cell activation by distinct mechanisms. *Mol. Cell. Biol.* **25**, 9543–9553 (2005). doi:10.1128/MCB.25.21.9543-9553.2005 Medline

25. F. Bennett, D. Luxenberg, V. Ling, I.-M. Wang, K. Marquette, D. Lowe, N. Khan, G. Veldman, K. A. Jacobs, V. E. Valge-Archer, M. Collins, B. M. Carreno, Program death-1 engagement upon TCR activation has distinct effects on costimulation and cytokine-driven proliferation: Attenuation of ICOS, IL-4, and IL-21, but not CD28, IL-7, and IL-15 responses. *J. Immunol.* **170**, 711–718 (2003). doi:10.4049/jimmunol.170.2.711 Medline

26. J. L. Riley, PD-1 signaling in primary T cells. *Immunol. Rev.* **229**, 114–125 (2009). doi:10.1111/j.1600-065X.2009.00767.x Medline

27. J. Yang, L. Liu, D. He, X. Song, X. Liang, Z. J. Zhao, G. W. Zhou, Crystal structure of human protein-tyrosine phosphatase SHP-1. *J. Biol. Chem.* **278**, 6516–6520 (2003). doi:10.1074/jbc.M210430200 Medline

28. J. M. Chemnitz, R. V. Parry, K. E. Nichols, C. H. June, J. L. Riley, SHP-1 and SHP-2 associate with immunoreceptor tyrosine-based switch motif of programmed death 1 upon primary human T cell stimulation, but only receptor ligation prevents T cell activation. *J. Immunol.* **173**, 945–954 (2004). doi:10.4049/jimmunol.173.2.945 Medline

29. T. Okazaki, A. Maeda, H. Nishimura, T. Kurosaki, T. Honjo, PD-1 immunoreceptor inhibits B cell receptor-mediated signaling by recruiting src homology 2-domain-containing tyrosine phosphatase 2 to phosphotyrosine. *Proc. Natl. Acad. Sci. U.S.A.* **98**, 13866–13871 (2001). doi:10.1073/pnas.231486598 Medline

30. L. E. Marengère, P. Waterhouse, G. S. Duncan, H.-W. Mittrücker, G.-S. Feng, T. W. Mak, Regulation of T cell receptor signaling by tyrosine phosphatase SYP association with CTLA-4. *Science* **272**, 1170–1173 (1996). doi:10.1126/science.272.5265.1170 Medline

31. C. E. Rudd, The reverse stop-signal model for CTLA4 function. *Nat. Rev. Immunol.* **8**, 153–160 (2008). doi:10.1038/nri2253 Medline

32. R. J. Greenwald, G. J. Freeman, A. H. Sharpe, The B7 family revisited. *Annu. Rev. Immunol.* **23**, 515–548 (2005). doi:10.1146/annurev.immunol.23.021704.115611 Medline

33. K. J. Oestreich, H. Yoon, R. Ahmed, J. M. Boss, NFATc1 regulates PD-1 expression upon T cell activation. *J. Immunol.* **181**, 4832–4839 (2008). doi:10.4049/jimmunol.181.7.4832 Medline

34. A. Hutloff, A. M. Dittrich, K. C. Beier, B. Eljaschewitsch, R. Kraft, I. Anagnostopoulos, R. A. Kroczek, ICOS is an inducible T-cell co-stimulator structurally and functionally related to CD28. *Nature* **397**, 263–266 (1999). doi:10.1038/16717 Medline

35. H. Wang, T. A. Kadlecek, B. B. Au-Yeung, H. E. S. Goodfellow, L. Y. Hsu, T. S. Freedman, A. Weiss, ZAP-70: An essential kinase in T-cell signaling. *Cold Spring Harb. Perspect. Biol.* **2**, a002279 (2010). doi:10.1101/cshperspect.a002279 Medline

36. M. Bergman, T. Mustelin, C. Oetken, J. Partanen, N. A. Flint, K. E. Amrein, M. Autero, P. Burn, K. Alitalo, The human p50csk tyrosine kinase phosphorylates p56lck at Tyr-505 and down regulates its catalytic activity. *EMBO J.* **11**, 2919–2924 (1992). Medline

37. W. Zhang, J. Sloan-Lancaster, J. Kitchen, R. P. Trible, L. E. Samelson, LAT: The ZAP-70 tyrosine kinase substrate that links T cell receptor to cellular activation. *Cell* **92**, 83–92 (1998). doi:10.1016/S0092-8674(00)80901-0 Medline

38. F. Pagès, M. Ragueneau, R. Rottapel, A. Truneh, J. Nunes, J. Imbert, D. Olive, Binding of phosphatidylinositol-3-OH kinase to CD28 is required for T-cell signalling. *Nature* **369**, 327–329 (1994). doi:10.1038/369327a0 Medline

39. X. Zang, P. Loke, J. Kim, K. Wojnoonski, L. Kusdra, J. P. Allison, A genetic library screen for signaling proteins that interact with phosphorylated T cell costimulatory receptors. *Genomics* **88**, 841–845 (2006). doi:10.1016/j.ygeno.2006.08.012 Medline

40. E. Hui, R. D. Vale, In vitro membrane reconstitution of the T-cell receptor proximal signaling network. *Nat. Struct. Mol. Biol.* **21**, 133–142 (2014). doi:10.1038/nsmb.2762 Medline

41. T. Yokosuka, W. Kobayashi, K. Sakata-Sogawa, M. Takamatsu, A. Hashimoto-Tane, M. L. Dustin, M. Tokunaga, T. Saito, Spatiotemporal regulation of T cell costimulation by TCR-CD28 microclusters and protein kinase C θ translocation. *Immunity* **29**, 589–601 (2008). doi:10.1016/j.immuni.2008.08.011 Medline

42. K. Choudhuri, J. Llodrá, E. W. Roth, J. Tsai, S. Gordo, K. W. Wucherpfennig, L. C. Kam, D. L. Stokes, M. L. Dustin, Polarized release of T-cell-receptor-enriched microvesicles at the immunological synapse. *Nature* **507**, 118–123 (2014). doi:10.1038/nature12951 Medline

43. R. Tian, H. Wang, G. D. Gish, E. Petsalaki, A. Pasculescu, Y. Shi, M. Mollenauer, R. D. Bagshaw, N. Yosef, T. Hunter, A.-C. Gingras, A. Weiss, T. Pawson, Combinatorial proteomic analysis of intercellular signaling applied to the CD28 T-cell costimulatory receptor. *Proc. Natl. Acad. Sci. U.S.A.* **112**, E1594–E1603 (2015). doi:10.1073/pnas.1503286112 Medline

44. A. O. Kamphorst, A. Wieland, T. Nasti, S. Yang, R. Zhang, D. L. Barber, B. T. Konieczny, C. Z. Daugherty, L. Koenig, K. Yu, G. L. Sica, A. H. Sharpe, G. J. Freeman, B. R. Blazar, L. A. Turka, T. K. Owonikoko, R. Pillai, S. S. Ramalingam, K. Araki, R. Ahmed, Rescue of exhausted CD8 T cells by PD-1–targeted therapies is CD28-dependent. *Science* 10.1126/science.aaf0683 (2017). 10.1126/science.aaf0683

45. L. Fehrenbacher, A. Spira, M. Ballinger, M. Kowanetz, J. Vansteenkiste, J. Mazieres, K. Park, D. Smith, A. Artal-Cortes, C. Lewanski, F. Braiteh, D. Waterkamp, P. He, W. Zou, D. S. Chen, J. Yi, A. Sandler, A. Rittmeyer; POPLAR Study Group, Atezolizumab versus docetaxel for patients with previously treated non-small-cell lung cancer (POPLAR): A multicentre, open-label, phase 2 randomised controlled trial. *Lancet* **387**, 1837–1846 (2016). doi:10.1016/S0140-6736(16)00587-0 Medline

46. S. J. Im, M. Hashimoto, M. Y. Gerner, J. Lee, H. T. Kissick, M. C. Burger, Q. Shan, J. S. Hale, J. Lee, T. H. Nasti, A. H. Sharpe, G. J. Freeman, R. N. Germain, H. I. Nakaya, H.-H. Xue, R. Ahmed, Defining $CD8^+$ T cells that provide the proliferative burst after PD-1 therapy. *Nature* **537**, 417–421 (2016). doi:10.1038/nature19330 Medline

47. R. He, S. Hou, C. Liu, A. Zhang, Q. Bai, M. Han, Y. Yang, G. Wei, T. Shen, X. Yang, L. Xu, X. Chen, Y. Hao, P. Wang, C. Zhu, J. Ou, H. Liang, T. Ni, X. Zhang, X. Zhou, K. Deng, Y. Chen, Y. Luo, J. Xu, H. Qi, Y. Wu, L. Ye, Follicular CXCR5-expressing $CD8^+$ T cells curtail chronic viral infection. *Nature* **537**, 412–428 (2016). doi:10.1038/nature19317 Medline

48. V. Mitaksov, S. M. Truscott, L. Lybarger, J. M. Connolly, T. H. Hansen, D. H. Fremont, Structural engineering of pMHC reagents for T cell vaccines and diagnostics. *Chem. Biol.* **14**, 909–922 (2007). doi:10.1016/j.chembiol.2007.07.010 Medline

49. X. Su, J. A. Ditlev, E. Hui, W. Xing, S. Banjade, J. Okrut, D. S. King, J. Taunton, M. K. Rosen, R. D. Vale, Phase separation of signaling molecules promotes T cell receptor signal transduction. *Science* **352**, 595–599 (2016). doi:10.1126/science.aad9964 Medline

50. G. P. O'Donoghue, R. M. Pielak, A. A. Smoligovets, J. J. Lin, J. T. Groves, Direct single molecule measurement of TCR triggering by agonist pMHC in living primary T cells. *eLife* **2**, e00778 (2013). doi:10.7554/eLife.00778 Medline

51. J. B. Huppa, M. Axmann, M. A. Mörtelmaier, B. F. Lillemeier, E. W. Newell, M. Brameshuber, L. O. Klein, G. J. Schütz, M. M. Davis, TCR-peptide-MHC interactions in situ show accelerated kinetics and increased affinity. *Nature* **463**, 963–967 (2010). doi:10.1038/nature08746 Medline

52. A. D. Edelstein, M. A. Tsuchida, N. Amodaj, H. Pinkard, R. D. Vale, N. Stuurman, Advanced methods of microscope control using μManager software. *J. Biol. Methods* **1**, 10 (2014). doi:10.14440/jbm.2014.36 Medline

53. P. Hof, S. Pluskey, S. Dhe-Paganon, M. J. Eck, S. E. Shoelson, Crystal structure of the tyrosine phosphatase SHP-2. *Cell* **92**, 441–450 (1998). doi:10.1016/S0092-8674(00)80938-1 Medline

54. A. Weiss, J. Schlessinger, Switching signals on or off by receptor dimerization. *Cell* **94**, 277–280 (1998). doi:10.1016/S0092-8674(00)81469-5 Medline

55. S. C. Meuer, O. Acuto, R. E. Hussey, J. C. Hodgdon, K. A. Fitzgerald, S. F. Schlossman, E. L. Reinherz, Evidence for the T3-associated 90K heterodimer as the T-cell antigen receptor. *Nature* **303**, 808–810 (1983). doi:10.1038/303808a0 Medline

56. B. A. Schodin, T. J. Tsomides, D. M. Kranz, Correlation between the number of T cell receptors required for T cell activation and TCR-ligand affinity. *Immunity* **5**, 137–146 (1996). doi:10.1016/S1074-7613(00)80490-2 Medline

57. M. W. Olszowy, P. L. Leuchtmann, A. Veillette, A. S. Shaw, Comparison of p56lck and p59fyn protein expression in thymocyte subsets, peripheral T cells, NK cells, and lymphoid cell lines. *J. Immunol.* **155**, 4236–4240 (1995). Medline

58. O. Acuto, F. Michel, CD28-mediated co-stimulation: A quantitative support for TCR signalling. *Nat. Rev. Immunol.* **3**, 939–951 (2003). doi:10.1038/nri1248 Medline

59. Y. D. Chung, M. D. Sinzinger, P. Bovee-Geurts, M. Krause, S. Dinkla, I. Joosten, W. J. Koopman, M. J. W. Adjobo-Hermans, R. Brock, Analyzing the homeostasis of signaling proteins by a combination of Western blot and fluorescence correlation spectroscopy. *Biophys. J.* **101**, 2807–2815 (2011). doi:10.1016/j.bpj.2011.09.058 Medline

60. M. Mkrtichyan, Y. G. Najjar, E. C. Raulfs, L. Liu, S. Langerman, G. Guittard, L. Ozbun, S. N. Khleif, B7-DC-Ig enhances vaccine effect by a novel mechanism dependent on PD-1 expression level on T cell subsets. *J. Immunol.* **189**, 2338–2347 (2012). doi:10.4049/jimmunol.1103085 Medline

61. C. Schaab, T. Geiger, G. Stoehr, J. Cox, M. Mann, Analysis of high accuracy, quantitative proteomics data in the MaxQB database. *Mol. Cell. Proteomics* **11**, 014068 (2012). doi:10.1074/mcp.M111.014068 Medline

62. M. J. Rosenbluth, W. A. Lam, D. A. Fletcher, Force microscopy of nonadherent cells: A comparison of leukemia cell deformability. *Biophys. J.* **90**, 2994–3003 (2006). doi:10.1529/biophysj.105.067496 Medline

63. G. Altan-Bonnet, R. N. Germain, Modeling T cell antigen discrimination based on feedback control of digital ERK responses. *PLOS Biol.* **3**, e356 (2005). doi:10.1371/journal.pbio.0030356 Medline

64. K. Okkenhaug, B. Vanhaesebroeck, PI3K in lymphocyte development, differentiation and activation. *Nat. Rev. Immunol.* **3**, 317–330 (2003). doi:10.1038/nri1056 Medline